

THREE-DIMENSIONAL SAR FROM CURVILINEAR APERTURES
IEEE 1996 NATIONAL RADAR CONFERENCE*

Kenneth Knaell
Carderock Division NSWC
Bethesda, Maryland, U.S.A.

ABSTRACT

Three-dimensional information content in radar data taken from suitably curved aperture paths is sufficient to allow useful 3D images to be produced by appropriate imaging techniques. The coherent CLEAN algorithm, the IMP algorithm, and maximum likelihood estimation have been used to produce 3D images from data obtained for two such scenarios.

The IMP algorithm in conjunction with likelihood extremization produces images free of sidelobe leakage effects found in the CLEAN algorithm. The CLEAN and IMP algorithms find use initiating likelihood extremization on or near its global maximum.

Dynamic range of such images appears dependent upon levels at which artifacts appear although valid scatterers are indicated below such levels. Artifacts appear to be a function of the image sidelobes determined by the aperture configuration. Reduction of this problem and methods to increase image size will extend the general usefulness of this technique.

1.0 INTRODUCTION

Three-dimensional(3D) information content in radar data taken from suitably curved aperture paths has been found sufficient for production of useful 3D images by iterative imaging techniques usually associated with two-dimensional image resolution enhancement. The coherent CLEAN algorithm, the IMP algorithm, and maximum likelihood(ML) estimation have yielded 3D images from data obtained for two such scenarios.

The importance of 3D information in target detection and identification is generally accepted and its relevance to radar has been documented (Steinberg, 1990). Stereoscopic viewing methods have been applied to synthetic aperture radar(SAR) ground image pairs to enhance interpretation (Fullerton, 1986). This type of information may also be of value for the determination of "hot spot" locations on military vehicles in need of suppression treatment for radar cross section reduction purposes.

A target consisting of a cubic arrangement of eight corner reflectors was rotated in rasterscan fashion to produce frequency diverse radar data distributed in azimuth and elevation as in Fig 1.1A. Decimation of this data in the patterns of Fig. 1.1 yielded subsets approximating those which could be obtained from single curvilinear sweeps through azimuth and elevation angle by

*Presented at the IEEE National Radar Conference, Ann Arbor, Michigan, 13-16 May 1996.

an airborne radar. Results of computer simulations and images from such subsets indicated the initial feasibility of this technique (Knaell, 1994; Knaell, 1995).

Subsequent datasets have been obtained from a helicopter borne radar of a ground target consisting of seven corner reflectors mounted upon a nine foot high tripod with reflectors placed around its base for ground delineation, Fig 1.2. Superimposed upon this is a projection of a 3D CLEAN image. (Perspectives for deep objects are not the same in these images.)

Results indicate that high resolution 3D images may be obtained from datasets generated by a radar in operational scenarios as illustrated in Fig. 1.3. This technique is well suited to the imaging of objects consisting of finite numbers of isolated scattering centers typical of man made objects.

2.0 IMAGE DECONVOLUTION

The coherent CLEAN algorithm has been shown to improve the clarity of high resolution SAR images by removal of sidelobes without the loss in resolution accompanying the use of tapered windows for such purposes (Steinberg, 1991). The use of the CLEAN algorithm to remove the clutter due to the large point spread function of curved aperture paths elevates the significance of this image enhancement technique to another level of importance in the generation of 3D images however. Without the use of a deconvolution or spectral estimation technique, 3D images formed from such apertures are nearly useless for visual purposes.

2.1 CLEAN STATISTICS

The residual peak, a , remaining after the n th iteration of CLEAN in an image consisting of one scatterer is:

$$a_{n+1} = a_n - g a_n \quad (1)$$

where g is the CLEAN gain factor and n the iteration number. The solution to this is:

$$a_n = a_0 e^{-gn} \quad (2)$$

For small gains the CLEAN algorithm first attenuates one scattering center to the level of a second and then alternates between these two. As this multiplicity increases to M multiple peaks the combined attenuation rate is reduced by that multiplicity. Thus for multiple scatterers the above becomes:

$$a_n = a_M e^{-gn/M} \quad (3)$$

In the absence of sidelobe leakage effects one thus expects the logarithm of amplitude generated by CLEAN to appear as in Fig. 2.1. Fig. 2.2 illustrates deviation from this behavior for an imaged object of eight scatterers. The eight equally bright scatterers produce an initial slope valid for this number which decreases to values characteristic of more scatterers. The reason for this behavior is mismatch in the form or position of the image response and the deconvolution function. This effect leaves a successively more distorted residue as the algorithm progresses. This persists even with ideal scatterers obtained from simulated data as a result of alignment error between the PSF and its image counterpart; this in turn produced by sidelobe leakage from neighboring scatterers.

2.2 THE IMP ALGORITHM

A solution to the sidelobe leakage problem is available in the IMP algorithm (Clarke, 1991). This algorithm may be compared to CLEAN with $g=1.0$ and with an additional optimization step per-

formed as each new scatterer is recorded. As each scatterer is revealed by a peak in the residue image function, it is incorporated into the accumulating ensemble of scatterers and their mutual adjustment accomplished by a minimization of a cost function in which biases of sidelobe leakage are absent. The usefulness of this algorithm for radar image generation is further enhanced by the fact that the cost function, in the form of the log-likelihood function introduced below, does not incur the expense of an image synthesis at each iteration in its optimization.

2.3 MAXIMUM LIKELIHOOD (ML) ESTIMATION

The multivariate Gaussian probability density for K uncorrelated variables, $\{F\}$, is:

$$P(\{F\}) = \frac{1}{2\pi\sigma^2} \exp \left\{ -\sum_0^K |D_k - F_k|^2 / 2\sigma^2 \right\} \quad (4)$$

If the expected data are the Fourier transform of an image, this represents the likelihood of that image given the data. The logarithm of this is the loglikelihood function:

$$\text{Loglikelihood} = \frac{1}{2\sigma^2} \sum_0^K |D_k - F_k|^2 \quad (5)$$

The term, $D_k - F_k$, is the difference between model data and real data for the k-th data point. The synthesized data is a function of model scatterer positions, scatterer amplitudes, and focusing parameters. Minimization of this function with respect to the aperture variables along with the scatterer parameters constitutes a useful autofocus technique. The IMP or CLEAN algorithms may be used as preprocessors to obtain initial scatterer parameters and the model order for likelihood maximization or the likelihood function may be considered the cost function in IMP.

3.0 IMAGERY

Diffraction limited images were produced by spherical backprojection of moderate bandwidth X-Band data. One hundred CLEAN iterations at a gain of -2db/step typically result in images of 12 to 20 db dynamic range, Fig. 3.1. Improvement in focus produced by ML optimization of 64 aperture elevation angles is apparent in Fig. 3.2. Apparent in stereo are tighter groupings of circles on the tripod and a flatter distribution of ground plane scatterers. These apertures are compared in Fig. 3.3 with the vertical deviation of the ML aperture from the input aperture magnified by a factor of 10 in order to make this difference visible on the graph.

The character of a preliminary IMP image is evident in Fig. 3.4. Although limited to a rank of 40 scatterers, this image shows a valid scatterer not present in the CLEAN image of Fig. 3.2. The ground truth for these images is Fig. 3.5.

A satisfactory viewer for the stereograms consists of two lenses of 6 inch focal length separated by 3.75 inches such as sold by Taylor-Merchant Corp. Circle diameters in the images are proportional to the square root of amplitude.

4.0 CONCLUSIONS

High resolution 3D SAR images have been produced from radar data limited to curvilinear apertures. Dynamic range of such images appears dependent upon the level at which artifacts appear although valid scatterers are indicated below such levels. Artifacts appear to be a function of the image sidelobes determined by the aperture configuration. Reduction of this problem and methods to increase image size will extend the general usefulness of this technique.

5.0 REFERENCES

I. J. Clarke, "Supervised Interpretation of Sampled Data Using Efficient Implementations of Higher-Rank Spectrum Estimation", In *"Advances in Spectrum Analysis and Array Processing"*, Vol II, Prentice Hall, Englewood Cliffs, New Jersey, 1991, Chap. 2, pp.65-121.

K.J. Fullerton, F. Leberl, and R.E. Marke, "Opposite-Side SAR Image Processing for Stereo Viewing", *Photogrammetric Engineering and Remote Sensing*, Vol. 52, No. 9, September 1986, pp1487-1498.

K. Knaell, "Three-Dimensional SAR from Curvilinear Apertures", *Proceedings SPIE*, Vol. 2230(1994), pp 120-134.

K. Knaell and G. P. Cardillo, "Radar Tomography for the Generation of Three-Dimensional Images", *IEE Proc. Radar, Sonar, Navig.*, April 1995, Vol. 142, No. 2, pp 54-60.

B.D. Steinberg and B. Kang, "Radar Detection Sensitivity as a Function of Target Dimensionality", *IEEE International Radar Conference, 1990*, Proceedings, p106.

B.D. Steinberg and H.M. Subbaram, *"Microwave Imaging Techniques"*, John Wiley and Sons, New York., 1991, Ch. 7.

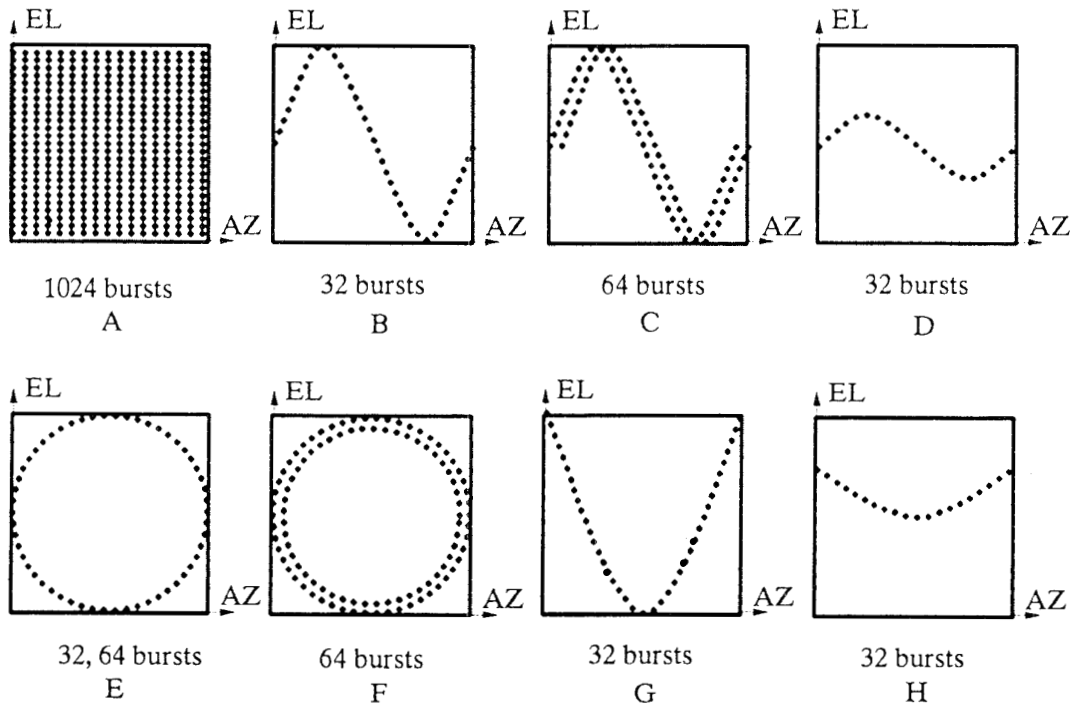


Fig. 1.1 Full Aperture and Derived Subsets

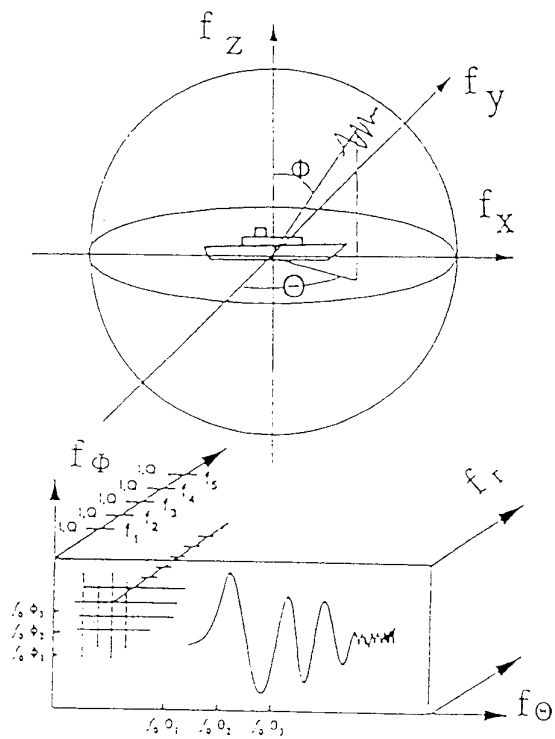
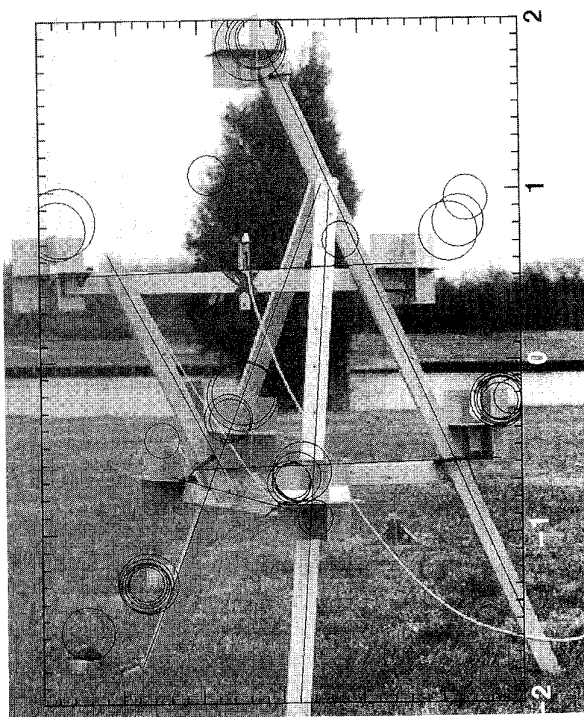


Fig. 1.2 Ground target for helicopter measurement. Fig. 1.3 Curvilinear aperture in target coordinates.

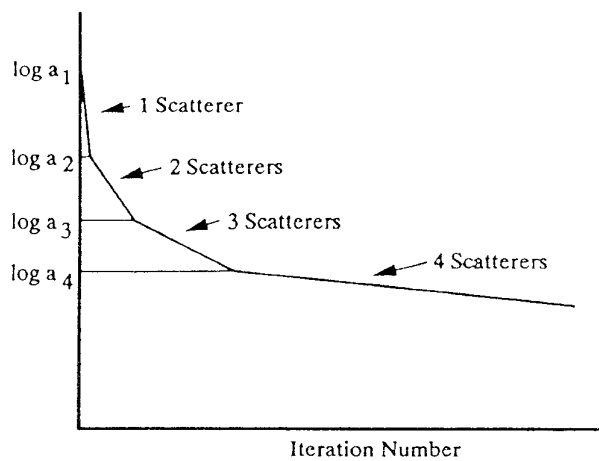


Fig. 2.1 Ideal CLEAN attenuation.

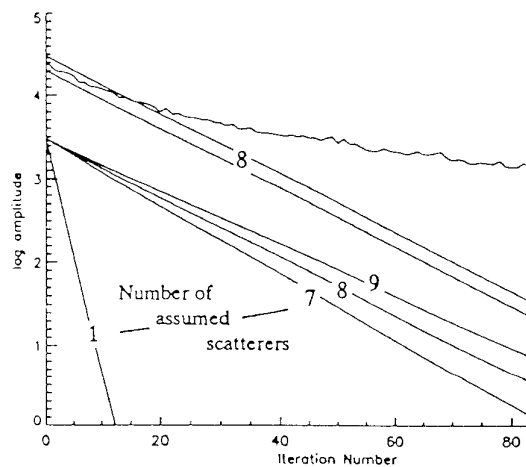


Fig. 2.2 Measured CLEAN attenuation for 8 scatterers.

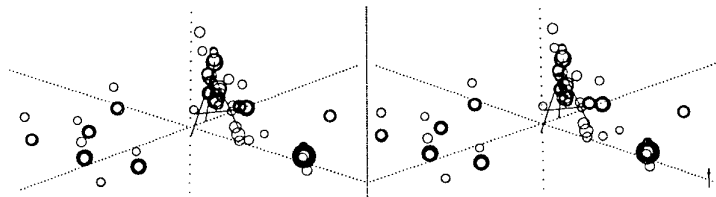


Fig. 3.1 CLEAN image, 100 iterations.

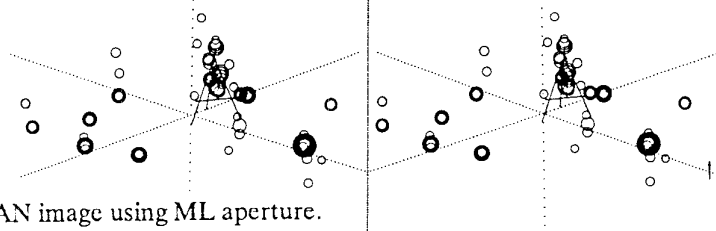


Fig. 3.2 CLEAN image using ML aperture.

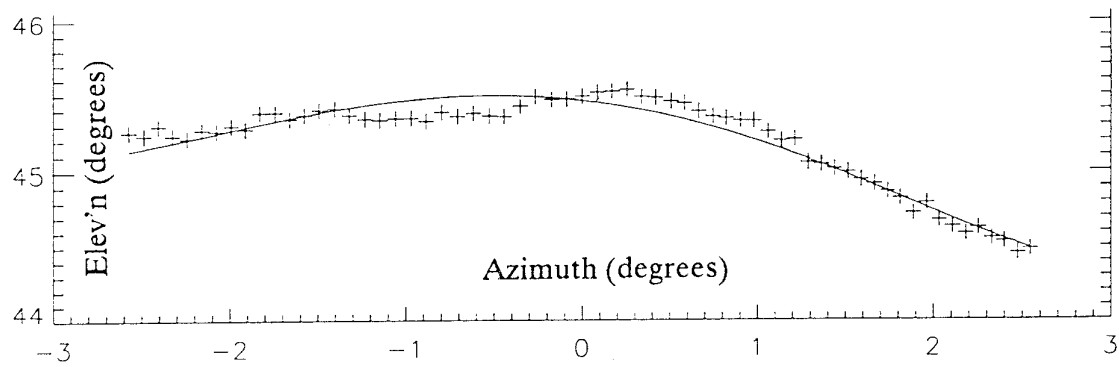


Fig. 3.3 First aperture (solid) and magnified ML aperture (points), see text.

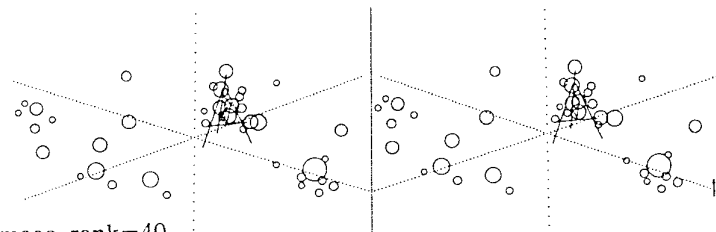


Fig. 3.4 IMP image, rank=40.

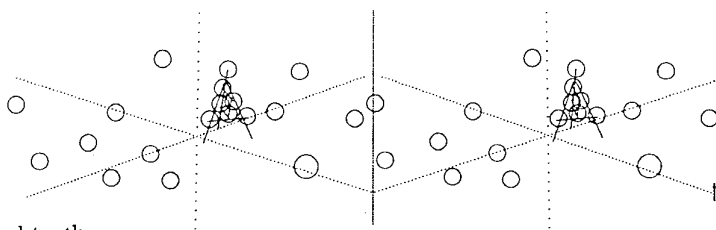


Fig. 3.5 Ground truth.

<-STEREO->